Quantitative and qualitative characterization of permafrost sites using surface waves

Hongwei Liu[1,2], Pooneh Maghoul[1] & Ahmed Shalaby[3]
[1]*Department of Civil, Geological and Mining Engineering– Polytechnique Montréal, Montréal, Québec, Canada*
[2]*KGS Groups, Winnipeg, Manitoba, Canada*
[3]Department of Civil Engineering, University of Manitoba, Winnipeg, Manitoba, Canada

GeoCalgary 2022 October 2-5
Reflection on Resources

ABSTRACT
The adverse effects of climate warming on the built environment in (sub)arctic regions are unprecedented and accelerating. According to Canada's Changing Climate Report (2019), in the Arctic regions, temperatures have been warming at approximately twice the rate of the rest of the world. This drastic trend in climate warming will no doubt affect permafrost temperatures and conditions, continued rise in greenhouse gas emissions, and further adding to the high cost of development in northern regions. Planning and design of climate-resilient northern infrastructure as well as predicting deterioration of permafrost from climate model simulations require characterizing permafrost sites accurately and efficiently. This paper presents a summary of the main results presented by Liu et al. (2022). In this paper, we propose a novel algorithm for analysis of surface waves to quantitatively estimate the physical and mechanical properties of a permafrost site. In-situ surface wave measurements can reveal the experimental dispersion relations of different Rayleigh waves from which relevant properties of a permafrost site can be derived by means of our proposed hybrid inverse and multi-phase poromechanical approach. Our proposed technique can be potentially used in early detection and warning systems to monitor infrastructure impacted by permafrost-related geohazards, and to detect the presence of layers vulnerable to permafrost carbon feedback and emission of greenhouse gases into the atmosphere.

RÉSUMÉ
Les effets néfastes du réchauffement climatique sur l'environnement bâti dans les régions (sub)arctiques sont sans précédent et s'accélèrent. Selon le Rapport sur le climat changeant du Canada (2019), dans les régions arctiques, les températures se sont réchauffées à environ deux fois le taux du reste du monde. Cette tendance drastique au réchauffement climatique affectera sans aucun doute les températures et les conditions du pergélisol, l'augmentation continue des émissions de gaz à effet de serre et augmentera encore le coût élevé du développement dans les régions du Nord. La planification et la conception d'infrastructures nordiques résilientes au climat ainsi que la prévision de la détérioration du pergélisol à partir de simulations de modèles climatiques nécessitent la caractérisation précise et efficace des sites de pergélisol. Cet article présente un résumé des principaux résultats présentés par Liu et al. (2022). Dans cet article, nous proposons un nouvel algorithme d'analyse des ondes de surface pour estimer quantitativement les propriétés physiques et mécaniques d'un site de pergélisol. Les mesures d'ondes de surface in situ peuvent révéler les relations de dispersion expérimentales de différentes ondes de Rayleigh à partir desquelles les propriétés pertinentes d'un site de pergélisol peuvent être dérivées au moyen de notre approche poromécanique hybride inverse et multiphase proposée. Notre technique proposée peut être potentiellement utilisée dans les systèmes de détection précoce et d'alerte pour surveiller les infrastructures touchées par les géorisques liés au pergélisol et pour détecter la présence de couches vulnérables à la rétroaction du carbone du pergélisol et à l'émission de gaz à effet de serre dans l'atmosphère.

1 INTRODUCTION

Permafrost is defined as the ground that remains at or below 0◦C for at least two consecutive years. The shallower layer of the ground in permafrost areas, termed as the active layer, undergoes seasonal freeze-thaw cycles. The thickness of the active layer depends on local geological and climate conditions such as vegetation, soil composition, air temperature, solar radiation and wind speed (Liu et al. 2019b).

Within the permafrost, the distribution of ice formations is highly variable. Ground ice can be present under distinctive forms including (1) pore ice, (2) segregated ice, and (3) ice-wedge. Pore water, which fills or partially fills the pore space of the soil, freezes in-place when the temperature drops below the freezing point (Porter et al. 2020). On the other hand, segregated ice is formed when water migrates to the freezing front and it can cause excessive deformations in frost-susceptible soils. Frost-susceptible soils, e.g. silty or silty clay soils, have relatively high capillary potential and moderate intrinsic permeability. During the winter months, ground ice expands as the ground freezes, and forms cracks in the subsurface (Liljedahl et al. 2016). Ice wedges are large masses of ice formed over many centuries by repeated frost cracking and ice vein growth.

Design and construction of structures on permafrost normally follow one of two broad principles which are based on whether the frozen foundation soil in ice-rich permafrost is thaw-stable or thaw-unstable. This distinction is determined by the ice content within the permafrost. Ice-rich permafrost contains ice in excess of

its water content at saturation and is thaw unstable. The construction on thaw-unstable permafrost is challenging and requires remedial measures since upon thawing, permafrost will experience significant thaw-settlement and suffer loss of strength to values significantly lower than that for similar material in an unfrozen state (Liu et al. 2019a). Consequently, remedial measures for excessive soil settlements or design of new infrastructure in permafrost zones affected by climate warming would require a reasonable estimation of the ice content within the permafrost (frozen soil). The rate of settlement relies on the mechanical properties of the foundation permafrost at the construction site. Furthermore, a warming climate can accelerate the microbial breakdown of organic carbon stored in permafrost and can increase the release of greenhouse gas emissions, which in return would accelerate climate change (Schuur et al. 2015).

Several in-situ techniques have been employed to characterize or monitor permafrost conditions. For example, techniques such as remote sensing (Bhuiyan et al. 2020; Witharana et al. 2020; Zhang et al. 2018), and ground penetrating radar (GPR) (Christiansen et al. 2016; Munroe et al. 2007; Williams et al. 2011) have been used to detect ice-wedge formations within the permafrost layers. Also, electrical resistivity tomography (ERT) has been extensively used to qualitatively detect pore-ice or segregated ice in permafrost based on the correlation between the electrical conductivity and the physical properties of permafrost (e.g. unfrozen water content and ice content) (Glazer et al. 2020; You et al. 2013). The apparent resistivity measurement by ERT is higher in areas having high ice contents (You et al. 2013); however, at high resistivity gradients, the inversion results become less reliable, especially for the investigation of permafrost base (Hilbich et al. 2009). Furthermore, in ERT investigations, the differentiation between ice and certain geomaterials can be highly uncertain due to their similar electrical resistivity properties (Kneisel et al. 2008). GPR has also been used for mapping the thickness of the active layer; however, its application is limited to a shallow penetration depth in conductive layers due to the signal attenuation and high electromagnetic noise in ice and water (Kneisel et al. 2008). It is worth mentioning that none of the above-mentioned methods directly characterizes the mechanical properties of permafrost layers.

Here, we present a hybrid inverse and multi-phase poromechanical approach for in-situ characterization of permafrost sites using surface wave techniques. The forward solver is used to numerically calculate the physics-based dispersion curves for both R1 and R2 wave modes given the soil properties. The inverse solver is used to inversely obtain the physical and mechanical properties of soils given the seismic measurements. In our method, we quantify the physical properties such as ice content, unfrozen water content, and porosity as well as the mechanical properties such as the shear modulus and bulk modulus of permafrost or soil layers. We also determine the depth of the permafrost table. The role of two different types of Rayleigh waves in characterizing the permafrost is presented based on an MASW seismic investigation in a field site located at SW Spitsbergen, Svalbard. Multiphase poromechanical dispersion relations are developed for the interpretation of the experimental seismic measurements at the surface based on the spectral element method. Our results demonstrate the potential of seismic surface wave testing accompanied with our proposed hybrid inverse and poromechanical dispersion model for assessment and quantitative characterization of permafrost sites.

2 METHOD

2.1 Methodology Overview

An overview of the proposed hybrid inverse and poromechanical approach for in-situ characterization of permafrost sites is summarized as follows: We can obtain the experimental dispersion relations for R1 and R2 Rayleigh wave types from the surface wave measurements. Then, we use the experimental dispersion of R2 waves to characterize the physical properties of the layers. A set of initial values, randomly selected and spanning the multidimensional parameter space ensures that soil parameters are not affected by a local minimum. Then the forward three-phase poromechanical dispersion solver is used to compute the theoretical dispersion relation of the R2 wave. Therefore, we can rank samples based on the L2 norm between the experimental and theoretical dispersion relations. Based on the ranking of each sample, the Voronoi polygons (Neighborhood sampling method) are used to generate better samples with a smaller objective function until the solution converges. We can select the best samples with the minimum loss function and obtain the most likely physical properties and thickness of the active layer, permafrost layer, and unfrozen ground. After obtaining the physical properties, the mechanical properties can be derived based on the dispersion relation of the R1 wave mode in a similar manner, as summarized in Figure 1h (optimization variables exclude the physical properties and the thickness of each layer in this process).

2.2 Identification of Rayleigh waves (R1 and R2) dispersion relations

From a poromechanical point of view, permafrost (frozen soil) is a multi-phase porous medium that is composed of a solid skeletal frame and pores filled with water and ice with different proportions. Here, we analyze the seismic wave propagation in permafrost based on the three-phase poroelastodynamic theory. Three types of P wave (P1, P2 and P3) and two types of S wave (S1, S2) coexist in three-phase frozen porous media. The P1 and S1 waves are strongly related to the longitudinal and transverse waves propagating in the solid skeletal frame, respectively, but are also dependent on the interactions with pore ice and pore water. The P2 and S2 waves propagate mainly within pore ice. Similarly, the P3 wave is due to the interaction between the pore water and the solid skeletal frame.

In this paper, a uniform frozen soil layer is used to show the propagation of different types of P and S waves and subsequently the formation of Rayleigh waves (R1

and R2) at the surface. It is assumed that an impulse load with a dominant frequency of 100 Hz is applied at the ground surface. The wave propagation analysis was performed in clayey soils by assuming a porosity (n) of 0.5, a degree of saturation of unfrozen water (Sr) of 50%, a bulk modulus (K) of 20.9 GPa and a shear modulus (G) of 6.85 GPa for the solid skeletal frame (Helgerud et al. 1999). The velocities of the P1 and P2 waves are calculated as 2,628 m/s and 910 m/s, respectively. The velocity of P3 wave (16 m/s) is relatively insignificant in comparison to P1 and P2 wave velocities. Similarly, the velocities of the S1 and S2 waves are calculated as 1,217 m/s and 481 m/s, respectively. Accordingly, the observed displacements measured at the ground surface with an offset from the impulse load ranging from 0 to 120 m are illustrated in Figure 1a. We found that the velocity of R1 and R2 is 1,150 m/s and 450 m/s, respectively, which is exactly the same as what we captured in Figure 1a. It is commonly known that the Rayleigh wave is slightly slower than the shear wave velocity and the ratio of Rayleigh wave and shear wave velocity ranges from 0.92-0.95 for Poisson's ratio greater than 0.3 (Kazemirad et al. 2013). From this analysis, we found the ratio of R1 and S1 wave velocity is around 0.93. Similarly, the ratio of R2 and S2 wave velocity is around 0.94. Therefore, we can conclude that R1 waves appear due to the interaction of P1 and S1 waves since the phase velocity of R1 waves is slightly slower than the phase velocity of S1 waves. Similarly, R2 waves appear due to the interaction of P2 and S2 waves since the phase velocity of R2 waves is also slightly slower than the phase velocity of S2 waves. Figures 1b illustrates the waveforms of R1 and R2 waves at the offset of 80 m. It can be seen that the R1 and R2 waves have a much larger amplitude than any other components (e.g. P1, P2, S1 and S2), which is also consistent with the typical understanding of Rayleigh wave. Figures 1c and 1d illustrate the appearance of two types of Rayleigh waves (R1 and R2) in a three-phase permafrost subsurface at 70 ms and 100 ms, respectively. Our results convincingly demonstrate that R1 waves appear due to the interaction of P1 and S1 waves and R2 waves appear due to the interaction of P2 and S2 waves. Briefly, the order of phase velocities of different waves propagating within the domain is as follows: P1>P2>S1>R1>S2>R2>P3.

The phase velocities of R1 and R2 waves are a function of physical properties (e.g. degree of saturation of unfrozen water, degree of saturation of ice, and porosity) and mechanical properties of the solid skeletal frame (e.g. bulk modulus and shear modulus). Figure 2d illustrates the effect of shear modulus and bulk modulus of the solid skeletal frame on the phase velocity of R1 and R2 waves. Similarly, Figure 2e illustrates the effect of porosity and degree of saturation of ice on the phase velocity of R1 and R2 waves. It can be seen that the phase velocity of the R1 wave is mostly sensitive to the shear modulus of the solid skeletal frame; it is also dependent on the bulk modulus, porosity, and degree of saturation of ice. On the other hand, the phase velocity of the R2 wave is almost independent of the mechanical properties of the solid skeletal frame (Figure 1d), while it is strongly affected by the porosity and degree of saturation of ice (Figure 2e). Our results also show that an increase in the degree of saturation of ice leads to an increase in the phase velocity of both types of Rayleigh waves. An increase in porosity leads to an increase in the phase velocity of R2. However, an increase in porosity may lead to either a decrease or an increase in the phase velocity of R1 wave, depending on the level of the degree of saturation of ice. Hence, we use the phase velocity of R2 waves identified by processing the seismic surface wave measurements to characterize the physical properties (e.g. porosity, degree of saturation of ice or degree of saturation of unfrozen water) of permafrost or soil layers.

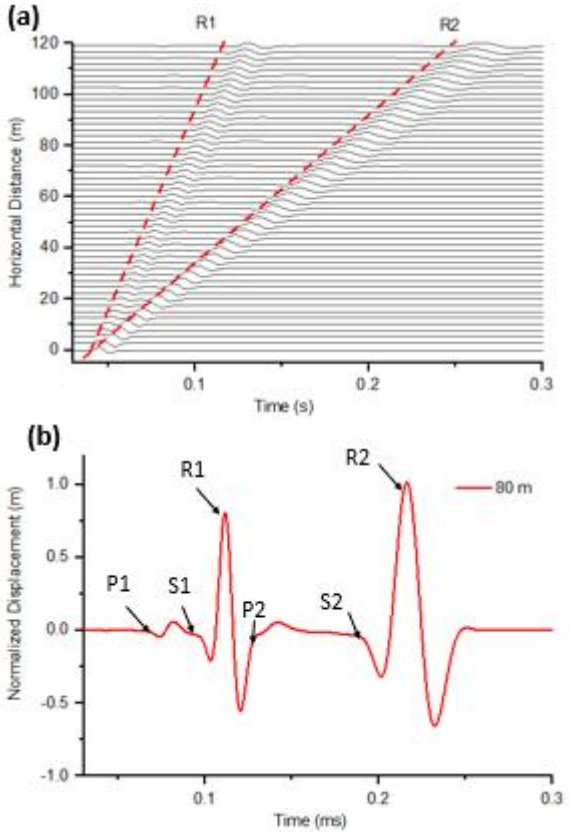

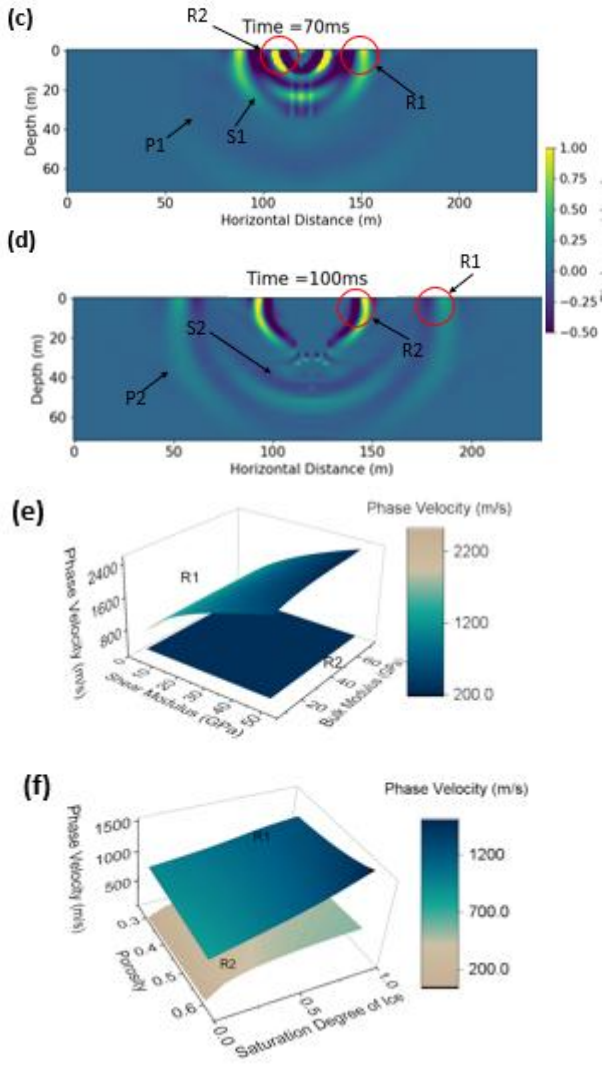

Figure 1. (a) Theoretical time-series measurements for R1 and R2 Rayleigh waves at the ground surface (b) Waveforms of R1, R2 and other wave modes at the offset of 80 m. (c) Displacement contour at time 70 ms. (d) Displacement contour at time 100 ms with the labeled R1 and R2 Rayleigh waves. (e) Effect of shear modulus and bulk modulus of the solid skeletal frame on phase velocity of R1 and R2 waves. (f) Effect of degree of saturation of ice on the phase velocity of R1 and R2 waves.

3 CASE STUDY FOR CHARACTERIZATION OF A PERMAFROST SITE USING SURFACE WAVE TECHNIQUE

The field experiment used in this study was performed by (Glazer et al. 2020) who aimed to study the effect of nearby glacial ice and surface watercourses on the formation of different ice-bearing sediments (development of permafrost) within the late Quaternary marine terraces. In this paper, the same experimental data collected by (Glazer et al. 2020) is used to demonstrate the inversion analysis based on R1 and R2 Rayleigh waves. The case study site is located at the Fuglebekken coastal area in SW Spitsbergen, Svalbard (77°00'30"N and 15°33'00"E). The study area has a thick layer of unconsolidated sediments that are suitable for near-surface geophysical investigations (Glazer et al. 2020). The unconsolidated sedimentary rock contains a high proportion of pore spaces; consequently, they can accumulate a large volume of pore-water or pore-ice. It was reported by (Szymanski et al. 2013) that this study site also contains a lot of coarse sandy soils and gravels based on the direct sampling methods at the top 15 cm. The direct sampling results also confirmed that the study site is very wet and the water table is very high (around 15 cm). From meteorological records, the mean annual air temperature (MAAT) at the testing site was historically below the freezing point, but more recently and due to a trend of climate warming, the MAAT recorded in 2016 is approaching 0℃ (Glazer et al. 2020). Glazer et al. (2020) performed both seismic surveys (MASW test) and electrical resistivity investigations at the site in September 2017 to study the evolution and formation of permafrost considering surface watercourses and marine terraces. The MASW test was performed by using 60 geophone receivers with a frequency of 4.5 Hz spaced at regular 2 m intervals. Figure 2a shows the location of the test site. Figures 2b, 2c and 2d show the test site with different soil types (silty, clayey and sandy sediment as well as gravels). Figure 2e illustrates the collected original seismic measurements at distances between 0 m and 120 m (hereafter referred to Section 1). The R1 and R2 Rayleigh waves are identified to obtain the experimental dispersion relations (Figures 2e and 2f). The phase velocity of R1 wave increases with frequency from 24 Hz to 80 Hz. The phase velocity of R2 wave decreases with frequency in the span of 18 Hz to 32 Hz. The largest wavelength is 22 m, calculated by the ratio of phase velocity of 404 m/s and a frequency of 18 Hz. The investigation depth in this study is focused on the first 11 m (based on the recommendation that the MASW investigation depth is roughly half of the maximum wavelength (Olafsdottir et al. 2018).The uncertainties due to the selection of the dispersion curve from the dispersion spectra have been considered. The dispersion curve is automatically selected initially based on the highest intensity in the dispersion spectra using the 'phase-shift method' in MASWave software (Olafsdottir et al. 2018). Then a 90% confidence interval (labeled as lower bound, highest intensity and upper bound, as shown in Figures 3f and 3g, is considered to study the uncertainties of the selection of dispersion curve to the inversion results.

In our simulations, the permafrost site is modeled as a three-layered system, consisting of an active layer at the surface followed by a permafrost layer on top of the third layer (permafrost or unfrozen ground, which is to be determined). The ERT results reported by Glazer et al. (2020) proved that the active layer is most likely completely unfrozen during the MASW testing performed in September. The degree of saturation of unfrozen water is considered 100% for the active layer in our study. The temperature of the permafrost layer remains below or at 0◦C all year round, but the volumetric ice content of the test site is unknown. Therefore, in our simulation, the

degree of saturation of unfrozen water in the permafrost layer is considered to be between 1% and 85% to be conservative. The degree of saturation of unfrozen water in the third layer is between 1%-100% (permafrost or unfrozen ground, which is to be determined). In our study, the third layer is assumed to be infinite. However, with the limited investigation depth constrained by the wavelength of the performed MASW tests, the inversion results beyond the maximum investigation depth are not considered in the paper. The porosity of all three layers is distributed between 0.1 and 0.7. We previously showed that the dispersion relation of the R2 wave is strongly dependent on the physical properties (e.g. porosity and degree of saturation of unfrozen water). Hence, the R2 dispersion relation (Figure 3d) is used first to determine the most probable distributions of porosity and degree of saturation of unfrozen water with depth. The other physical properties such as degree of saturation of ice, volumetric water content and volumetric ice content can also be obtained by knowing porosity and degree of saturation of unfrozen water.

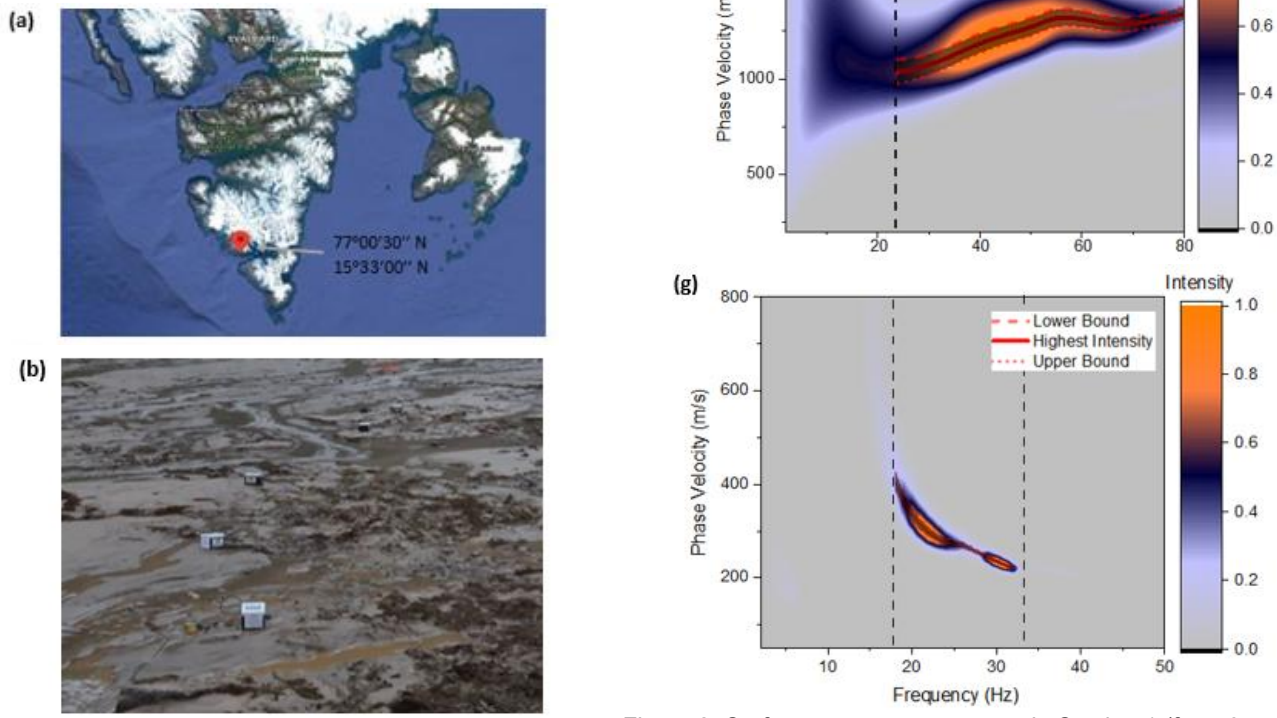

Figure 2. Surface wave measurement in Section 1 (from 0 m to 120 m). (a) Study area in Holocene, Fuglebekken, SW Spitsbergen. (b) Testing site with clayey silt soils. (c) Testing site with gravels and sands. (d) Testing site with patterned ground. (e) Waveform data from the measurements at different offsets in horizontal distance. (f) Experimental dispersion image for R1 wave. (g) Experimental dispersion image for R2 wave.

The mechanical properties of the solid skeletal frame in each layer are then obtained using the R1 wave dispersion relation. The mechanical properties can be then used to determine whether the permafrost site is ice-rich. In fact, the thin ice lenses can not be detected directly when the thickness of ice lenses is smaller than 1/2 wavelength generated by low frequency seismic

waves. However, the mechanical properties (e.g. shear modulus and bulk modulus) of permafrost reveal the mineral composition of the soil and soil type (Leclaire et al. 1994), which is valuable in the classification of ice-rich permafrost or even detection of whether the permafrost layer is prone to greenhouse gases carbon dioxide and methane emission to the atmosphere.

Figure 3a shows the distribution of the degree of saturation of unfrozen water with depth in Section 1. Our results show that the active layer has a thickness of about 1.5 m. The predicted permafrost layer (second layer) has a nearly 32% of degree of saturation of unfrozen pore water. Figure 3b shows the degree of saturation of ice with depth. The degree of saturation of ice in the permafrost layer (second layer) ranges from 67% to 71%. Figure 3c illustrates the porosity distribution with depth. The porosity is around 0.60 in the first layer (active layer), from 0.40 to 0.47 in the second layer (permafrost) and from 0.56 to 0.59 in the third layer. Figure 3d and 3e show the predicted mechanical properties of the solid skeletal frame (shear modulus and bulk modulus) in each layer. It was reported by Szyman´ski et al. (2013) that this study site also contains a lot of coarse sandy soils, gravels as well as around 20% silty clay based on the direct sampling methods at the top 15 cm. The predicted shear modulus and bulk modulus for the solid skeletal frame in the permafrost layer (second layer) are about 13 GPa and 12.7 GPa, which are in the range for silty-clayey soils and are also consistent with the local soil types described by (Szymanski et al. 2013). The predicted shear modulus and bulk modulus for the solid skeletal frame in the third layer are about 4 GPa and 10 GPa, which are in the range for clayey soils. Figure 3f and 3g show the comparison between the numerical and experimental dispersion relations for R2 and R1 waves, respectively. The numerical predictions show good agreement with the experimental dispersion curves for both R1 (RMS value of 1.9) and R2 (RMS value of 4.7) waves.

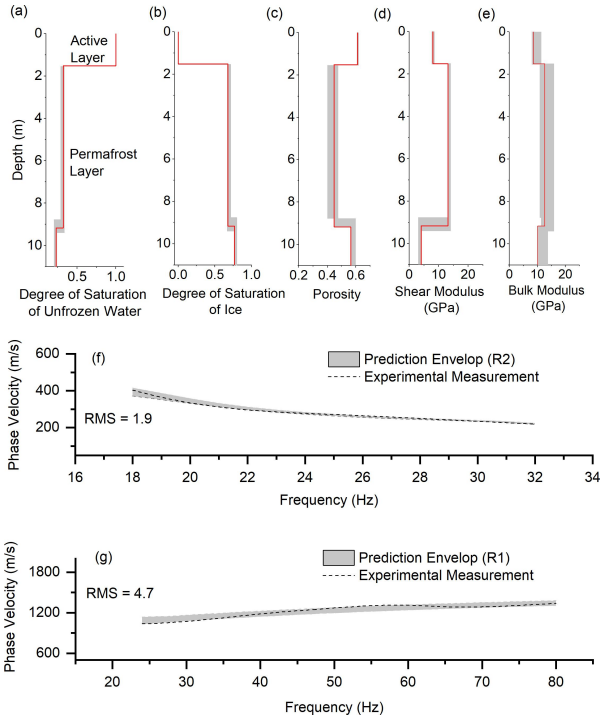

Figure 3. Surface wave inversion results for 0 m to 120 m. (a) Degree of saturation of unfrozen water, (b) Degree of saturation of ice, (c) Porosity distribution, (d) Shear modulus of solid skeletal frame, (e) Bulk modulus of solid skeletal frame, (f) Experimental and numerical dispersion curves for R2 wave, (g) Experimental and numerical dispersion curves for R1 wave.

4 DISCUSSION AND CONCLUSIONS

We developed a hybrid inverse and multi-phase poromechanical approach to quantitatively estimate the physical and mechanical properties of a permafrost site. The identification of two distinctive types of Rayleigh waves in the surface wave field measurements in permafrost sites is critical for the quantitative characterization of the layers. The identification of the R2 wave allows the quantitative characterization of the physical properties of soil layers independently without making assumptions of the mechanical properties of the layers. This approach simplifies the inversion of the multi-layered three-phase poromechanical model since the dependent optimization variables are largely reduced. The inversion results from the R2 wave dispersion relation can be further used in the characterization of the mechanical properties of soil layers based on the R1 wave dispersion relation. This also increases the stability and convergence rate of the inversion solver and makes the analysis more efficient than the joint inversion analysis.

The proposed hybrid inverse and multi-phase poromechanical approach can potentially be used for the design of an early warning system for permafrost by means of an active or passive seismic test. The seismic noise from traffic can generate stress waves as they travel on the permafrost foundation. Pre-installed geophones can be used to capture the propagation of R1 and R2 waves. By applying the proposed signal processing approach, we can estimate the physical and mechanical properties of permafrost for monitored sites. The early warning system can provide long-term tracking of permafrost conditions particularly when the ice content or mechanical properties of permafrost approach critical values.

REFERENCES

Bhuiyan, K., Witharana, C. and Liljedahl, K. 2020. Use of Very High Spatial Resolution Commercial Satellite Imagery and Deep Learning to Automatically Map Ice-Wedge Polygons across Tundra Vegeta- tion Types. In: Journal of Imaging 6.12, p. 137

Christiansen, H. Matsuoka, H. and Watanabe, T. 2016. Progress in understanding the dynam- ics, internal structure and palaeoenvironmental potential of ice wedges and sand wedges. In: Permafrost and Periglacial Processes 27.4, pp. 365–376.

Couture, N. and Pollard, W. 2017. A Model for Quantifying Ground-Ice Volume, Yukon Coast, Western Arctic Canada. In: Permafrost and Periglacial Processes 28.3, pp. 534–542.

Glazer, M. 2020. Spatial distribution and controls of permafrost development in non-glacial Arctic catchment over the Holocene, Fuglebekken, SW Spitsbergen". In: Geomorphology, p. 107128.

Hauck, C. 2013. New concepts in geophysical sur- veying and data interpretation for permafrost terrain. In: Permafrost and Periglacial Processes 24.2, pp. 131–137.

Hilbich, C. 2009. Applicability of electrical resistiv- ity tomography monitoring to coarse blocky and ice-rich permafrost landforms. In: Permafrost and Periglacial Processes 20.3, pp. 269–284.

Kneisel, C. 2008. Advances in geophysical meth- ods for permafrost investigations. In: Permafrost and periglacial processes 19.2, pp. 157–178.

Liljedahl, A. 2016. Pan-Arctic ice-wedge degrada- tion in warming permafrost and its influence on tundra hydrology. In: Nature Geoscience 9.4, pp. 312– 318.

Liu, H. Maghoul, P. and Shalaby, A. 2019. Optimum insulation design for buried utilities subject to frost action in cold regions using the Nelder-Mead algorithm. In: International Journal of Heat and Mass Transfer, pp. 613–639.

Liu, H. Maghoul, P. and Shalaby, A. 2019. Thermo-hydro-mechanical model- ing of frost heave using the theory of poroelasticity for frost-susceptible soils in double-barrel culvert sites. In: Transportation Geotechnics, p. 100251.

Liu, H. Maghoul, P. and Shalaby, A. 2022. Seismic physics-based characterization of permafrost sites using surface waves. The Cryosphere, 16(4), 1157-1180.

Mackay, J. 1972. The world of underground ice. In: Annals of the Association of American Geographers 62.1, pp. 1–22.

Marescot, L. 2013. Assessing reliability of 2D resistiv- ity imaging in mountain permafrost studies using the depth of investigation index method". In: Near Surface Geophysics 1.2, pp. 57–67.

Munroe, J. 2007. Application of ground-penetrating radar imagery for three-dimensional visualisation of near- surface structures in ice-rich permafrost, Barrow, Alaska. In: Permafrost and Periglacial Processes 18.4, pp. 309–321.

Porter, J and Opel, J. 2020. Recent advances in paleoclimatological studies of Arctic wedge-and pore-ice stable-water isotope records. In: Permafrost and Periglacial Processes.

Scapozza, C. 2011. Internal structure and permafrost distribution in two alpine periglacial talus slopes, Valais, Swiss Alps. In: Geomorphology 132.3-4, pp. 208– 221.

Schuur, E. 2015. Climate change and the per- mafrost carbon feedback. In: Nature 520.7546, pp. 171–179.

Kanevskiy M.Z. Shur Y. Jorgenson M.T. 2011. Permafrost. In: Singh V.P., Singh P., Haritashya U.K. (eds) Encyclo- pedia of Snow, Ice and Glaciers. Encyclopedia of Earth Sciences Series.

Williams, K. and Haltigin, T. and Pollard, WH. 2011. Ground Penetrating Radar Detection of Ice Wedge Geometry: Implications for Climate Change Monitoring. In: AGUFM 2011, pp. C41C–0420.

Witharana, C. 2020. Understanding the synergies of deep learning and data fusion of multispectral and panchromatic high resolution commercial satellite im-agery for automated ice-wedge polygon detection . In: ISPRS Journal of Photogrammetry and Remote Sensing 170, pp. 174–191.

You, Y. 2013. Application of electrical resistivity tomography in investigating depth of permafrost base and permafrost structure in Tibetan Plateau. In: Cold Regions Science and Technology 87, pp. 19–26.

Zhang, W. 2018. Deep convolutional neural net- works for automated characterization of arctic ice-wedge polygons in very high spatial resolution aerial imagery. In: Remote Sensing 10.9, p. 1487.